KLOE/KLOE-2

The KLOE/KLOE-2 Collaboration at the LNF

D. Babusci, G. Bencivenni, C. Bloise (Resp.), F. Bossi, G. Capon (Ass.), P. Ciambrone, E. Czerwinski (Bors. PD), E. Dane' (Art. 23), E. De Lucia, P. de Simone, D. Domenici (Art. 23), J. Dong (Bors. EU), G. Felici, G. Fortugno (Tecn.), S. Giovannella, F. Happacher, E. Iarocci (Ass.)*, M. Iannarelli (Tecn.), J. Lee-Franzini (Ass), B. Leverington (Bors. PD), M. Martini (Ass)**, S. Miscetti, V. Patera (Ass.)*, G. Pileggi (Tecn.), B. Ponzio (Tecn.), R. Rosellini (Tecn.), F. Roukoutakis (Bors. EU), P. Santangelo, A. Saputi (Tecn.), I. Sarra (Dott.), F. Sborzacchi (Tecn.), B. Sciascia, A. Sciubba (Ass)*, E. Turri (Tecn.), G. Venanzoni.

In Collaboration with "LNF-SEA"
A. Balla, G. Corradi, U. Denni, A. Frani, M. Gatta, C. Paglia, G. Papalino
and "LNF SPAS"
S. Cerioni

*Also Dipartimento di Scienze di Base ed Applicate per l'Ingegneria, "Sapienza" University, Rome, Italy
**Also Dipartimento di Scienze e Tecnologie applicate,"Guglielmo Marconi" University, Rome, Italy

1 Introduction

The operation of the KLOE detector at DAΦNE continued during the year, except for the summer shutdown in July-August, in order to follow the machine studies providing the measurements of the luminosity, background levels, beam energy and beam position at the interaction region (IP). In August, the Amadeus Collaboration inserted a thin carbon target inside KLOE to collect data on kaon-nucleus interactions. Data taking for nuclear physics went on, mostly during nights and weekends, from November, with 100 pb^{-1} of integrated luminosity that should increase by a factor of three the data sample of K-N interactions previously selected from the 2.5 fb^{-1} of KLOE data. From the machine running, several results have been reached by the accelerator experts: i) with 102 bunches (1.1 A of electrons and 0.8 A positrons) and crab-waist sextupoles at half strength, DAΦNE operated at $1.4{\cdot}10^{32}$ cm^{-2} s^{-1}, with 4 pb^{-1} delivered in 12 hours; ii) in these conditions the luminosity is almost linear with current; iii) there is significantly scope for further luminosity improvements increasing current, an issue linked to the consolidation program planned for the 6-month shutdown started in December; iv) the expected performance increasing current is 2.0-2.5 fb^{-1} delivered in 250 running days assuming 50% global efficiency. Such results confirmed the program for DAΦNE consolidation, and running starting from June 2013. During the winter shutdown KLOE-2 will proceed with the installation of the upgrades, inner tracker and calorimeters, whose construction and test have been mostly finalized during the year, as presented in Sec.2-3. Detector installation and integration on the beam pipe is a crucial task both, for the importance of IP alignment and cooling for the DAΦNE performance, and for the impact on the operation of the detectors. Most of the procedures have been studied and tested on a mockup; cabling and cooling systems are being finalized.

Several analyses have been completed, i) on the hadronic cross section, Sec.4, ii) on the η production from γ–γ fusion [1)], iii) on the $\eta \to \pi\pi\gamma$ decays [2)], iv) on the U-boson searches, Sec.5, and other physics studies have been started as doctoral theses in Italy, Poland, and Sweden, reported in Sec.7.

2 The KLOE-2 inner tracker

Tracking detectors based on the Gas Electron Multiplier (GEM) technology have been used so far to equip forward regions of experiments at hadron machines (LHCb, COMPASS, TOTEM) fully exploiting their excellent rate capability (to 1 MHz/mm^2). At DAΦNE, where radiation flux is well below such a scale, the unique lightness of the GEM detector suggested the R&D for a cylindrical GEM, whose material budget could be kept lower than 2% of X_0. This feature is of utmost importance in KLOE-2, to limit the multiple scattering of low-momentum particles, photon conversions and K_S regeneration.

KLOE-2 is the first experiment using the GEM technology with a cylindrical geometry, developed at the LNF within the CERN RD51 Collaboration, aiming for technological advances of Micropattern Gas Detectors. The construction of the Inner Tracker (IT) has started in mid 2011; since then three layers have been completed and construction of the fourth (last) layer started in November 2012. Each layer is a triple-GEM detector composed by five concentric cylindrical electrodes: the cathode, to set the drift field, the 3 GEM foils for electron multiplication, and the anode that is also the readout circuit (Fig. 1,left). The IT is composed by four concentric CGEM

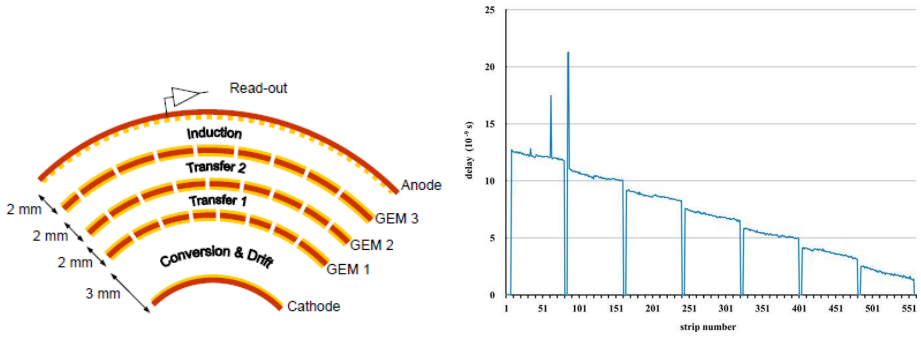

Figure 1: Cross-section of the triple-GEM cylindrical detector (left); Delay time measured for the V-view strips of half an anode foil of the second CGEM layer (right).

layers at radii from 13 cm, to preserve the K_S-K_L quantum interference region, to 20.5 cm, imposed by the KLOE DC inner wall, at 25 cm. The total active length for all layers is 70 cm. The anode readout of each CGEM is patterned with longitudinal X strips, 650 μm pitch, interleaved, on the same substrate and at the same level, with pads connected through internal vias to form V strips at an angle within 25°÷27° and with 650 μm pitch, for a total of about 30,000 FEE channels. The insertion of the IT is expected to improve by a factor of three the vertex resolution close to the interacton region, IP [3].

A dedicated readout system has been developed within the KLOE-2 collaboration. The Front-End Electronics is based on the new GASTONE ASIC [4], a 64 channels chip composed by four different stages: a charge preamplifier with 20 mV/fC sensitivity, a shaper, a leading-edge discriminator with a programmable threshold and a monostable stretcher of the digital signal, to synchronize with the KLOE Level1 trigger. GASTONE boards are one of the three elements of the IT data acquisition system together with the general interface boards (GIB) and the readout driver (ROD). The GIB board is based on a Xilinx Virtex 4FX Field Programmable Gate Array (FPGA) with an embedded IBM Power PC (PPC405) running at 300MHz. It has been designed to set up the front-end chip parameters, deliver the power supply and download data from a maximum of eight GASTONE. Data are then delivered from the 2 Gb/s optical port of the GIB board to the

ROD, which performs a first-level event-building, transfers data from GIBs to a VME CPU-board sending data to the online farm.

The IT project has been finalized after 3 years of intense R&D, from 2008 to 2010, with several prototypes built and tested with X-rays, cosmic-ray muons and pion beams at CERN. The three main stages have been: i) the construction and complete characterization of a full-scale CGEM prototype [5]; ii) the study of the readout system with a planar XV GEM chamber operated also in magnetic field, from 0.4-1.5 T, at the RD51 CERN-SPS facility [6]; iii) the construction and characterization of a large-area planar GEM realized with the new single-mask photolitografic technique [7]. The CGEM operation in magnetic field (B orthogonal to E) has been studied with 150 GeV/c pion beams, using two different gas mixtures at a gain of $\sim 10^4$: Ar/CO_2 (70/30) and $Ar/i\text{-}C_4H_{10}$(90/10). Spatial resolution in the bending plane increases with the magnetic field due to the Lorentz force spreading the charge over the readout plane.The resolution in the bending plane measured at 0.52 T (the value of the KLOE magnetic field) is $\sigma_{r\phi} \sim 200$ μm. Spatial resolution in the transverse direction to the bending plane is $\sigma_z \sim 350$ μm, insensitive to the magnetic field. Due to IT dimension, R&D was needed for a new GEM manufacturing procedure. The TE-MPE-EM CERN group produced GEM foils of unprecedented size (up to 50x100 cm^2) using single-mask electro-chemical etching of the micro-holes. Exploiting the intrinsic lightness of GEM foils (50 μm thick polyimide doubly clad with 2 μm copper films) and their extreme flexibility, we managed to manufacture a cylindrical GEM foil with only 2 mm wide overlap gluing region. The (Ar/iC_4H_{10}) gas mixture has been chosen after testing several alternatives (either Argon or Helium based mixtures), taking into account the most important operating parameters. In the cylindrical triple-GEM detector all the electrodes are made of polyimide foils. The uniformity of GEM holes, directly affecting the gain, has been measured over a surface as large as 70x30 cm^2. The anode quality check has been perfomed with 100 ps precision: the strip can be regarded as a transmission line and its length and possible damages can be evaluated by measuring the delay of the reflected input signal [8]. Fig. 1 (right) shows the distribution of the delay time measured for the V-view strips of half an anode foil of the second CGEM layer: the peaks represent shorts in the readout strips. After quality controls, the construction of the detector starts with the splicing of three separate foils to obtain a single electrode with dimensions of about 100x70 cm^2. The splicing is performed by distributing an epoxy glue (Araldite 2011) along the overlap between foils (2 mm wide) and then pressing the foils with a vacuum bag on a machined assembly table, for the 24 hours epoxy curing cycle. This large electrode foil is wrapped around an aluminum cylindrical mold, glued on a 2 mm wide overlap and finally enveloped in a vacuum bag. Two fiberglass rings are glued at the ends of the barrel, acting as spacers between electrodes, and as mechanical support. The surface of the mold is covered by a PTFE film, providing a low-friction surface, allowing the GEM to be extracted without damages. The cathode and the anode cylindrical electrodes are manufactured with a similar process, the only difference with respect to the GEM electrodes is that they are both reinforced with a 3 mm thick honeycomb structure coupled with thin external skins: 50 μm kapton foil for the cathode and 90 μm carbon foil for the anode. The assembly of the final detector is performed by inserting one into the other the cylindrical electrodes, starting by the anode and ending with the cathode. To this extent a dedicated machine has been built. The machine allows the insertion of the electrodes with a ~ 100 μm axial alignment over a length of about 1.5 m. The detector is then sealed at both ends to ensure gas tightness.
The three innermost CGEM layers of the Inner Tracker have been built, all of them tested in current mode with 5.9 keV X-rays, and equipped with GASTONE FEE.

While constructing the second CGEM layer, during DAΦNE commissioning, the beam pipe at the interaction region reached temperatures much higher than expected ($> 50°$C). For this reason on the second layer we made tests of operation at increasing temperatures showing some instability for T $> 35°$-$40°$C, due to the mechanical relaxation of the GEM electrodes. Although DAΦNE

operation at normal temperature was resumed since then, a cooling system for the interaction region was designed and tested to keep the temperature below 30°C. Moreover, to cope with possible accidents causing the mechanical relaxation of GEM foils, the third and the fourth CGEM layers have been built introducing between GEM electrodes a 300 μm support grid made of PEEK, a clean organic thermoplastic polymer(Fig. 2).

Figure 2: The PEEK grid is fixed on the kapton outside the GEM foil active area with epoxy glue.

To validate CGEM construction we have used cosmic-ray muons and a ^{90}Sr source that has been used to check each HV sector. Muon tracks at the cosmic ray stand have beem used for the measurement of cluster efficiency and spatial resolution. A test stand has been setup at the LNF with the final high voltage supply system, GASTONE, GIB and ROD boards. While testing the second CGEM layer, a correlated noise of the order of 10% was observed, analougously to what noticed for the first time on LHCb-GEMs. It has been explained as cross-talk due to the capacitive coupling between GEM3$_{bottom}$ and the readout plane. In events with large charge deposit, the current on the common GEM3$_{bottom}$ can induce signals on all the strips facing the GEM3 HV sector, originating "splash" events with high hit multiplicity. These events can be strongly suppressed by the insertion of a blocking capacitor (BC): with suitable tuning of the resistor R and capacitor C, the current induced on GEM3$_{bottom}$ flows through the BC rather than through the detector. Afterwards BCs have been mounted on all CGEM layers, the same solution adopted for the LHCb-GEMs.

In conclusion, after three years of R&D which has demonstrated the feasibility of cylindrical triple-GEM detector (CGEM) with an XV readout providing $\sigma_{r\phi} \sim 200$ μm and $\sigma_z \sim 350$ μm, completion of the KLOE-2 Inner Tracker is expected in January 2013. In fact, the three innermost CGEM layers have been built and the construction of the fourth has started. The IT insertion inside the KLOE apparatus and the integration with the DAΦNE beam pipe is planned during spring 2013.

3 Calorimeters for the KLOE upgrade

The QCALT calorimeter has been realized mostly to increase the KLOE acceptance for photons from neutral and radiative kaon decays in the drift chamber (DC). In fact, those photons crossing the DAΦNE beam pipe region can be lost due to the interactions with the focusing magnets or the beam pipe support. The calorimeters, on both sides of the IP, cover a total of 2 out of 3.6 m of the DC internal length (Fig.3, left). Fig.3, right, shows the half QCALT calorimeters whose construction has been completed in December 2012. They are constituted by 12 trapezoidal units,

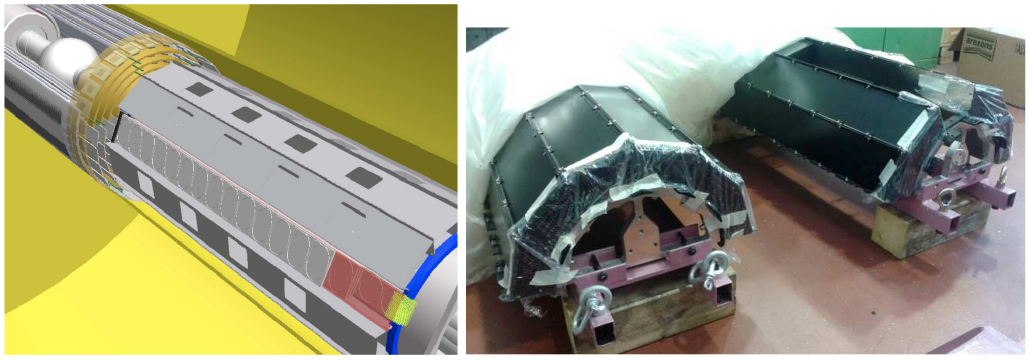

Figure 3: Inner tracker and QCALT calorimeter on the DAΦNE beam pipe (left) and half QCALT calorimeters (right).

5 layers each, with scintillator tiles interleaved with tungsten planes, for a total depth of 5.5 X_0. Each of the 18 tiles assembled in one layer has been machined to place one optical WLS fiber for light transport to a silicon photomultiplier (SiPM) of 1.2 mm diameter, at one end of the calorimeter, for a total of 2000 channels. SiPMs are custom device prepared in collaboration with the Advansid company, soldered on alumina PCBs, one PCB for each calorimeter module (80 channels). The alumina has been chosen to ensure a planarity better than 0.1 mm, and good heat dissipation. Such precision planarity is needed for optical coupling between PCB and fiber holder, mounted at the end of each module. As shown in Fig.3, right, one of the modules is kept free for the insertion of the LET (Low Energy Tagger) calorimeter, which is used as $\gamma\gamma$ tagger [9].

The electronic service of the LNF has developed custom electronics to manage the signals from many channels (Fig.4). The on–detector board contains pre-amplifiers and voltage regulator; a multifunction NIM board supplies the V_{bias} to the photodetectors with a precision of 2 mV and a stability at the level of 0.03 permill.

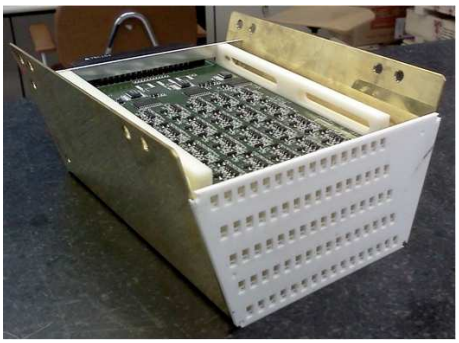

Figure 4: Cards with voltage regulators and readout circuits for the SiPMs that are mounted on the alumina (white) layer.

During construction, any single layer has been tested using a ^{90}Sr source to check all of the optical couplings between fibers and scintillator tiles. The result on the uniformity in light response was at the 10% level, fully compatible with the attenuation length of the fibers (WLS

multicladding, 1 mm diameter fibers produced by Bicron).

Tooling for QCALT installation on the beam pipe has been designed and is being realized. It consists of a mechanical system prepared to place half QCALT below beam pipe moving the other half on top of it. When the two halves are in contact, a screw system, both on modules and on steel rings, closes the calorimeter. The tooling also include a rotation system, allowing each calorimeter to reach the final angular position imposed by the LET detector.

Test of final QCALT electronics is in progress, including i) the check of the HV regulators to control their functionality, precision and stability in voltage setting; ii) a pulse test, in collaboration with the LNF Electronic Service, to check the discriminator thresholds; iii) the test of final FEE chain, with PCBs and DAQ system separately operated using both laser distributor and calorimeter modules.

The calorimeter at low polar angle, CCALT, is made by 96 LYSO crystals readout by silicon photomultipliers (SiPM). Calorimeter characterization has been obtained with the beam test at the LNF facility using 100 MeV electrons. The results on time resolution, $\sigma(t) \simeq$ 250 ps, is adequate to deal with the background rates observed in the DAΦNE interaction region, and the spatial resolution of 2-3 mm (at $\sim$15 cm from the IP) will improve event reconstruction by additional constraints on the kinematical fits. The CCALT position on the beam pipe and the calorimeter

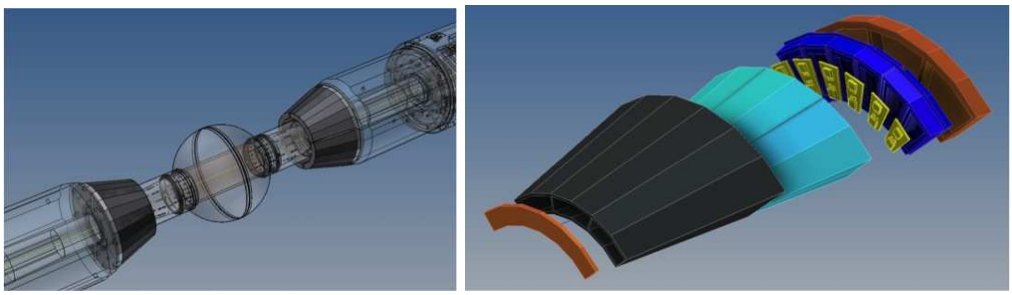

Figure 5: CCALT position on the DAΦNE beam pipe (left), and the components, PVC ring, mechanical structure, LYSO crystals, PCBs, PVC closing cap, and PVC support (right)

modularity are shown in Fig.5. In year 2012 both, the detector, and the FEE elements have been realized, including,

- LYSO crystals, produced by SICCAS in China,
- SiPMs, produced by Advansid in Italy,
- PCBs,
- mechanical structure,
- PVC holders for the readout cards containing both, SiPMs, and calibration LEDs.

The readout cards are being mounted. Crystal quality has been checked with a ^{22}Na source and each LYSO element wrapped in reflective Tyvek layers for optical decoupling from the others. A final test with the assembled crystals is scheduled before the calorimeter installation on the beam pipe, by mid March 2013.

4 Results on hadron physics

The analysis of the ISR $\mu\mu\gamma$ sample for the measurement of the hadron vacuum polarization contribution to muon anomaly, has been finalized and the paper submitted to PLB at end of 2012. Most of the analysis procedure is reported on the 2011 Activity Report (this series).

We summarize recent, final results, mostly on systematics and background subtraction relating to the $\mu\mu\gamma$ spectrum. Event selection includes:

- reconstruction of at least two tracks of opposite sign, with origin at the IP and polar angle satisfying $50° < \theta < 130°$. The momenta satisfy $p_\perp > 160$ MeV or $|p_z| > 90$ MeV, to ensure good reconstruction and efficiency;
- polar angle $\theta_{\mu\mu}$ of the the dimuon system ($\mathbf{p}_{\mu\mu} = \mathbf{p}_+ + \mathbf{p}_-$) satisfying $|\cos\theta_{\mu\mu}| < \cos(15°)$;
- computed mass for the two observed particles, as obtained from kinematical constraints assuming ISR $xx\gamma$ events, in the range $80 < m_x < 115$ MeV;
- PID estimator, $L_\pm$, which uses time of flight information and energy deposit of each charged particle in the calorimeter, compatible with muon hypothesis at least for one track.

Residual $e^+e^-\gamma$, $\pi^+\pi^-\gamma$ and $\pi^+\pi^-\pi^0$ backgrounds are evaluated by fitting the observed m_x spectrum with a superposition of Monte Carlo simulation (MC) distributions describing signal and $\pi^+\pi^-\gamma$, $\pi^+\pi^-\pi^0$ backgrounds, and a distribution obtained from data for the $e^+e^-\gamma$ background. In the ρ mass region, the fractional $\pi^+\pi^-\gamma$ yield in the $\mu\mu\gamma$ acceptance region is about 15% of the sample. To improve the MC description of the low energy m_x tail of $\pi^+\pi^-\gamma$ events in the muon peak, we apply a data/MC resolution correction, function of s_μ. This correction is evaluated from a high–purity sample of $\phi \to \pi^+\pi^-\pi^0$ events, with the results shown in Fig.6.

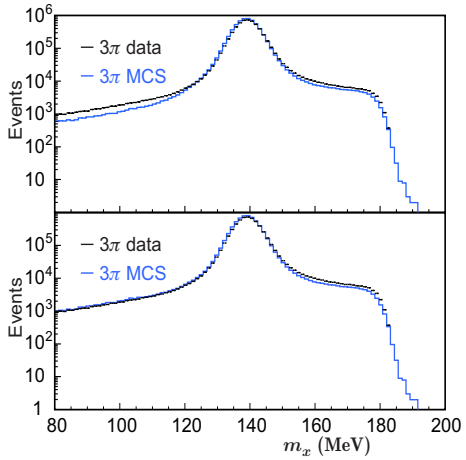

Figure 6: Data and MC m_x distributions for the $\pi^+\pi^-\pi^0$ control sample, before (upper) and after (lower) resolution correction.

Contributions from $e^+e^- \to e^+e^-\mu^+\mu^-$ and $e^+e^- \to e^+e^-\pi^+\pi^-$ processes are evaluated using the `Nextcalibur` [10] and `Ekhara` [11] MC generators. After analysis cuts, the $e^+e^- \to e^+e^-\pi^+\pi^-$ process is found to be negligible, while the $e^+e^- \to e^+e^-\mu^+\mu^-$ background contribution is between 0.6% and 0.1%, in the low $M^2_{\mu\mu}$ region and is subtracted from the data spectrum. Systematic errors in the background subtraction include: (*i*) errors on the parameters from the fit

procedure: these decrease monotonically from 0.7% to 0.1% with respect to s_μ; (*ii*) the uncertainty on the data/MC resolution corrections: about 1% in the ρ mass region, smaller at higher s_μ, negligible at lower s_μ values; (*iii*) the uncertainty on the $e^+e^- \to e^+e^-\mu^+\mu^-$ process: about 0.4% at low s_μ values, rapidly falling to 0.1% for $s_\mu > 0.5\,\mathrm{GeV}^2$. The correctness of the background estimate has been checked by two independent methods.

- We perform a kinematic fit of the two track events assuming it is a $\mu\mu\gamma$ state. The χ^2 value obtained is used as discriminant variable, instead of m_x, in the fitting procedure described above;
- we improve the π-μ separation by use of m_x, applying a quality cut on the helix fit for both tracks. This cut reduces the dipion background in the dimuon signal region by more than a factor of two.

The background fractions obtained for both cases are in good agreement with the standard procedure.

The differential $\mu^+\mu^-\gamma$ cross section is obtained from the observed event count $N_{\rm obs}$ and background estimate $N_{\rm bkg}$, as

$$\frac{\mathrm{d}\,\sigma_{\mu\mu\gamma}}{\mathrm{d}\,s_\mu} = \frac{N_{\rm obs} - N_{\rm bkg}}{\Delta s_\mu}\,\frac{1}{\epsilon(s_\mu)\,\mathcal{L}}. \tag{1}$$

where $\mathcal{L}$ is the integrated luminosity from Ref. [12] and $\epsilon(s_\mu)$ the selection efficiency. Figure 7 top, shows the measured $\mu^+\mu^-\gamma$ cross section compared with the QED calculations to NLO, using

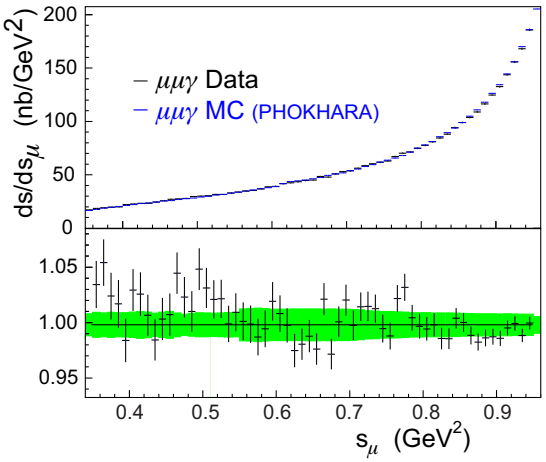

Figure 7: Top. Comparison of data and MC results for $\mathrm{d}\,\sigma_{\mu\mu\gamma}/\mathrm{d}\,s_\mu$. Bottom. Ratio of the two spectra. The green band shows the systematic error.

the MC code `Phokhara` [13]. Figure 7 bottom, shows the ratio between the two differential cross sections. The green band indicates the systematic uncertainty, experimental and theoretical, of the measured cross section. The average ratio, using only statistical errors, is 0.9981 ± 0.0015, showing a good agreement within the quoted systematic uncertainties.

From the bin-by-bin ratio between our published [14] $\pi^+\pi^-\gamma$, and the $\mu^+\mu^-\gamma$ differential cross sections described above, we obtain the bare cross section $\sigma^0_{\pi\pi(\gamma)}$ (inclusive of FSR, with VP effects removed) which is used in the dispersion integral for computing $\Delta^{\pi\pi}a_\mu$. Figure 8 shows the

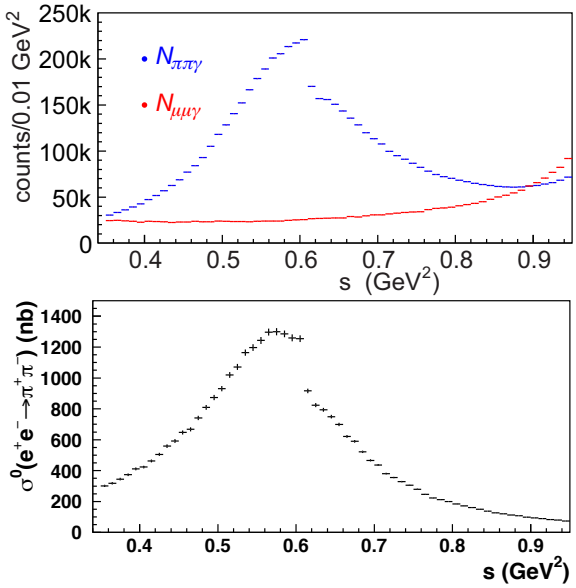

Figure 8: Square invariant mass distributions of $\pi^+\pi^-\gamma$ (blue) and $\mu^+\mu^-\gamma$ (red) events after background subtraction and data/MC corrections (top); the bare cross section from the $\pi^+\pi^-\gamma/\mu^+\mu^-\gamma$ ratio (bottom).

$\pi^+\pi^-\gamma$ and $\mu^+\mu^-\gamma$ event spectra after background subtraction and data/MC corrections (top) and the bare cross section $\sigma^0_{\pi\pi(\gamma)}$ (bottom). Systematic uncertainties on $\sigma^0_{\pi\pi(\gamma)}$ are smaller than the individual uncertainty on $\pi\pi\gamma$ and $\mu\mu\gamma$ due to correlation between the two measurements [15].

The dispersion integral for $\Delta^{\pi\pi}a_\mu$ is computed as the sum of the values for $\sigma^0_{\pi\pi(\gamma)}$ times the kernel $K(s)$, times $\Delta s = 0.01$ GeV^2 :

$$\Delta^{\pi\pi}a_\mu = \frac{1}{4\pi^3}\int_{s_{min}}^{s_{max}} \mathrm{d}\, s\, \sigma^0_{\pi\pi(\gamma)}(s)\, K(s)\ , \tag{2}$$

where the kernel is given in in Ref. [16].

Equation 2 gives $\Delta^{\pi\pi}a_\mu = (385.1 \pm 1.1_{\rm stat} \pm 2.6_{\rm exp} \pm 0.8_{\rm th}) \times 10^{-10}$ in the interval $0.35 < M^2_{\pi\pi} < 0.95\,\mathrm{GeV}^2$.

This result, with comparable total experimental uncertainty and a theoretical error reduced by about 70% with respect to our previous measurements [14], confirms the current discrepancy between the standard model prediction and the experimental value of a_μ.

5 Searches for U–boson

Some models of physics beyond the SM predict the existence of light neutral vector particles (called U–bosons) mediator of new gauge interactions under which ordinary matter is uncharged [17, 18]. Motivated by astrophysical arguments, their mass, M_U, is expected to be of order 1 GeV or lighter [19, 20]. Coupling of SM particles with the U is possible via kinetic mixing between the U and the ordinary photon [21], regulated by a dimensionless parameter ϵ, expected to be of order $\epsilon \sim 10^{-3}$ or lower.

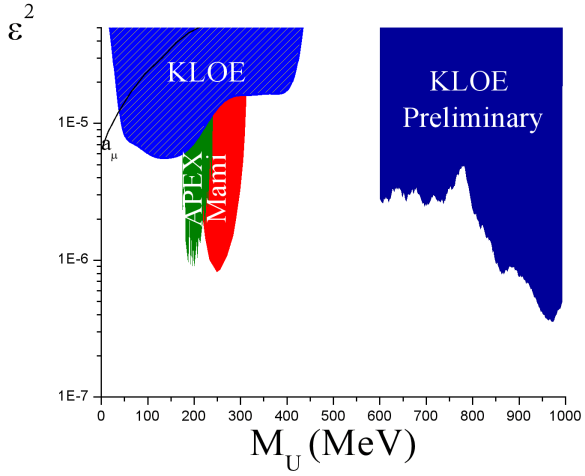

Figure 9: KLOE-2 limit in the plane M_U–ϵ^2. Results are shown for the $\phi \to \eta e^+e^-$ analysis and for the $e^+e^- \to \mu^+\mu^-\gamma$ one. The results from the APEX and MAMI-A1 experiments are also shown

These new particles can be observed as sharp resonances at M_U in the invariant mass distribution of charged lepton or pion pairs in reactions of the type $e^+e^- \to l^+l^-\gamma$ or $V \to Pl^+l^-$, where V (P) stands for any vector (pseudoscalar) meson, and $l^\pm$ can be muons, electrons or charged pions.

KLOE has searched for U boson production in both modes, using $\phi \to \eta e^+e^-$ events (a), and $e^+e^- \to \mu^+\mu^-\gamma$ events (b).

As for reactions (a), a first paper has been published [22] in which the presence of the η meson was tagged using its $\pi^+\pi^-\pi^0$ decays; a second paper has been subsequently issued [23] in which also the $3\pi^0$ decay channel of the η was used. In both cases a sample corresponding to 1.7 fb^{-1} of data at the ϕ peak was used; no evidence of the U boson is found, and the exclusion plot, in the interval $30 < M_U < 400$ MeV, has been obtained (Fig. 9).

Reaction (b) was studied on the sample used for the measurement of the ratio, $R = \sigma(e^+e^- \to \pi^+\pi^-)/\sigma(e^+e^- \to \mu^+\mu^-)$, presented in the previous section, exploiting the precision MC simulation of the QED process $e^+e^- \to \mu\mu\gamma$ reported in Fig. 7. The exclusion plot is obtained using the CL_S technique. The preliminary result shown in Fig. 9 covers the mass region $600 < M_U < 1000$ MeV and is currently being extended to 500 MeV.

If the hidden symmetry is broken by the Higgs mechanism, there is the possibility of the existence also of a non SM higgs-type particle, the h'. This can be produced together with the U–boson in reactions of the type $e^+e^- \to Uh'$ (the so called $higgs' - stralhung$ process). Then, if the h' is ligther than the U its lifetime becomes long, giving rise to event of the type $e^+e^- \to l^+l^- + missing\ energy/momentum$. These have been searched by KLOE, in the hypothesis $l = \mu$ in both, on-peak, and off-peak data. Again, no evidence of signal is found.

Results of the last two analyses are still preliminary. They are expected to be finalized in year 2013.

6 Doctoral theses completed in year 2012

1. Ivano Sarra, Tor Vergata University, Rome, Italy *Search for a dark force mediator in the $\phi \to \eta e^+ e^-$ decay at KLOE*; Supervisors: Prof. P. Picozza, Dr. S. Giovannella and Dr. S. Miscetti

2. Michal Silarski, Jagiellonian University of Krakow, Poland *Search for CP symmetry violation in the decay of K_S mesons using the KLOE detector*; Supervisor: Prof. P. Moskal

3. Cecilia Taccini, Roma-3 University, Rome, Italy *Measurement of η meson production in $\gamma\gamma$ interactions and $\Gamma(\eta \to \gamma\gamma)$ with the KLOE detector*; Supervisors: Prof. F. Ceradini and Dr. F. Nguyen

7 Ongoing Doctoral theses

1. Izabela Balwierz-Pytko, Jagiellonian University of Krakow, Poland *Study of K_S regeneration in the berillium beam pipe and in the carbon fiber wall of the drift chamber of the KLOE detector for the measurement of the cross sections at kaon momenta close to 100 MeV*; Supervisor: Prof. P. Moskal

2. Li Caldeira Balkestahl, Uppsala University, Sweden *Study of the $\eta \to \pi^+\pi^-\pi^0$ Dalitz plot with the KLOE detector for improving sensitivity on the light-quark mass ratio*; Supervisor: Dr. A. Kupsc

3. Francesca Curcianello, Messina University, Italy *Study of the $e^+e^- \to \mu\mu\gamma$ process with the KLOE detector to search for Dark photons*; Supervisors: Prof. G. Giardina, Dr. G. Mandaglio and Dr. G. Venanzoni

4. Veronica De Leo, Messina University, Italy *Study of the $e^+e^- \to \mu\mu\gamma$ process with the KLOE detector for probing vacuum polarization effects*; Supervisors: Prof. G. Giardina, Dr. G. Mandaglio and Dr. G. Venanzoni

5. Lena Heijkenskjld, Uppsala University, Sweden *Study of the $\omega \to \pi^+\pi^-\pi^0$ Dalitz plot with the KLOE detector for testing ChPT predictions*; Supervisor: Dr. A. Kupsc

6. Matteo Mascolo, Tor Vergata University, Rome, Italy *Study of the $e^+e^- \to \pi^0 e^+ e^-$ process with the KLOE detector for the measurement of the transition form factor*; Supervisors: Prof. R. Messi, Dr. D. Moricciani and Dr. D. Babusci

7. Ivan Prado Longhi, Roma-3 University, Rome, Italy *Study of the $\pi^0\pi^0$ production in $\gamma\gamma$ interactions with the KLOE detector for the measurement of the two-pion invariant mass distribution and the comparison with ChPT predictions*; Supervisors: Prof. F. Ceradini and Dr. A. Passeri

8. Jaroslaw Zdebik, Jagiellonian University of Krakow, Poland *Study of the $\phi \to \eta e^+ e^-$ Dalitz decays using KLOE data*; Supervisors: Prof. P. Moskal and Dr. S. Giovannella

8 Papers

1. D. Babusci, H. Czyz, F. Gonnella *et al. On the possibility to measure the $\pi^0 \to \gamma\gamma$ decay width and the $\gamma * \gamma \to \pi^0$ transition form factor with the KLOE-2 experiment* Eur. Phys. J. **C72** (2012) 1917

2. F. Archilli *et al.* (KLOE-2), *Search for a vector gauge boson in phi meson decays with the KLOE detector*, Phys. Lett. **B706** (2012) 251

3. D. Babusci *et al.* (KLOE), *Measurement of* $\Gamma(\eta \to \pi^+\pi^-\gamma)/\Gamma(\eta \to \pi^+\pi^-\pi^0)$ *with the KLOE Detector*, Phys. Lett. **B718** (2013) 910

4. D. Babusci *et al.* (KLOE-2), *Measurement of* η *meson production in* $\gamma\gamma$ *interactions and* $\Gamma(\eta \to \gamma\gamma)$ *with the KLOE detector*, J. of High Energy Phys. **1301** (2013) 119

5. G. Bencivenni, E. Czerwinski, E. De Lucia *et al.*, *A Time Domain Reflectometer with 100 ps precision implemented in a cost-effective FPGA for the test of the KLOE-2 Inner Tracker readout anodes*, Nucl. Inst. & Meth. **A698** (2013) 185

9 Talks and Conference Proceedings

1. S. Giovannella *et al.*, (KLOE-2) *KLOE searches on Dark Matter*, Talk at the Les Recontres de Physique de la Vallee d'Aoste, February 26-March 3 (2012), La Thuile, Italy

2. I. Sarra *et al.*, *Ricerca di Dark forces a KLOE*, Talk at the Incontri di Fisica della Alte Energie, IFAE 2012, April 11-13 (2012), Ferrara, Italy

3. A. Saputi *et al.*, *QCALT: a tile calorimeter for KLOE-2*, Talk at the 12th Pisa Meeting on Advanced Detectors, May 20-26 (2012), La Biodola, Italy

4. S. Giovannella *et al.*, *CCALT: a crystal calorimeter for the KLOE-2 experiment*, Talk at the 12th Pisa Meeting on Advanced Detectors, May 20-26 (2012), La Biodola, Italy

5. D. Domenici *et al.*, *Production and test of first layers of the KLOE-2 inner tracker*, Talk at the 12th Pisa Meeting on Advanced Detectors, May 20-26 (2012), La Biodola, Italy

6. E. Czerwinski *et al.*, (KLOE-2) *KLOE results on flavour physics*, Talk at the Fourth Capri Workshop on Theory, Phenomenology and Experiments on flavour physics, June 11-13 (2012), Capri, Italy

7. F. Bossi *et al.*, (KLOE-2) *Recent results from KLOE-2* , Talk at the 7th International Workshop on Chiral Dynamics, CD12, August 6-10 (2012), Newport News, Virginia, USA

8. I. Sarra *et al.*, (KLOE-2) *U-boson search at KLOE-2* , Talk at the International Workshop on Dark forces at Accelerators, DARK2012, October 16-19 (2012), Frascati, Italy

9. E. De Lucia *et al.*, *Production and test of first layers of the KLOE-2 inner tracker*, Talk at the 2012 Nucl. Sc. Symp. and Medical Imaging Conf., NSS/MIC 2012, Oct 19-November 3 (2012), Anaheim, California, USA

10. S. Miscetti, *Hadronic Physics at KLOE/KLOE-2* , Seminar at the Thomas Jefferson Lab, December 19th 2012, Newport News, Virginia, USA

11. M. Cordelli *et al.*, *Test and Simulation of a LYSO+APD matrix with a tagged Photon Beam from 40-MeV to 300-MeV*, J. Phys. Conf. Ser. **404** (2012) 012027; Proceedings of the 15th International Conference on Calorimetry in High Energy Physics (CALOR 2012)

12. C. F. Redmer *et al.*, (KLOE-2) *Measurement of* $\eta' \to \eta\pi\pi$ *with KLOE and KLOE-2*, EPJ Web Conf. **37** (2012) 09030; Proceedings of the 12th International Workshop on Meson Production, Properties and Interaction (MESON 2012)

13. Li Caldeira Balkestahl *et al.*, (KLOE-2) *Study of the $\eta \to \pi^+\pi^-\pi^0$ Dalitz plot with the KLOE detector*, EPJ Web Conf. **37** (2012) 09002; Proceedings of the 12th International Workshop on Meson Production, Properties and Interaction (MESON 2012)

14. M. Silarski *et al.*, (KLOE-2) *Search for the $K_s \to 3\pi^0$ decay with the KLOE detector*, EPJ Web Conf. **37** (2012) 05004 ; Proceedings of the 12th International Workshop on Meson Production, Properties and Interaction (MESON 2012)

15. F. Nguyen *et al.*, (KLOE-2) *Results and prospects on light meson spectroscopy with KLOE/KLOE-2*, Nucl. Phys. Proc. Suppl. **225-227** (2012) 121; Proceedings of the 8th International Workshop on e^+ e^- Collisions from Phi to Psi (PHIPSI 11)

16. P. Lukin *et al.*, (KLOE-2) *KLOE measurement of e^+ $e^- \to \pi\pi(\gamma)$ with initial state radiation and the $\pi\pi$ contribution to the muon anomaly*, Nucl. Phys. Proc. Suppl. **225-227** (2012) 265; Proceedings of the 8th International Workshop on e+ e- Collisions from Phi to Psi (PHIPSI 11)

17. A. De Santis *et al.*, (KLOE-2) *Recent results on CP and CPT tests at KLOE*, PoS **HQL2012** (2012) 018; Proceedings of 11th International Conference on Heavy Quarks and Leptons (HQL 2012)

18. F. Nguyen *et al.*, (KLOE-2) *Hadron physics at KLOE/KLOE-2*, AIP Conf.Proc. **1441** (2012) 347; Proceedings of the 19th International Conference on Particles and Nuclei (PANIC 11)

References

1. D. Babusci et al. (KLOE-2 Collaboration), JHEP **1301**, 119 (2013), 1211.1845
2. D. Babusci et al. (KLOE Collaboration), Phys.Lett. **B718**, 910 (2013), 1209.4611
3. F. Archilli et al. (KLOE-2 Collaboration) (2010), 1002.2572
4. A. Balla, G. Bencivenni et al., Nucl.Instrum.Meth. **A604**, 23 (2009)
5. G. Bencivenni, S. Cerioni et al., NSS CR 2008. IEEE **6**, 4666 (2007)
6. A. Balla, G. Bencivenni et al., Nucl.Instrum.Meth. **A628**, 194 (2011), 1003.3770
7. M. Alfonsi, G. Bencivenni et al., Nucl.Instrum.Meth. **A617**, 151 (2010)
8. G. Bencivenni, E. Czerwinski et al., Nucl.Instrum.Meth. **698**, 185 (2013)
9. D. Babusci, C. Bini, P. Ciambrone et al., Nucl.Instrum.Meth. **A617**, 81 (2010), 0906.0875
10. F.A. Berends et al., Comput.Phys.Commun. **136**, 148 (2001), hep-ph/0011031
11. H. Czyz, E. Nowak-Kubat, Phys.Lett. **B634**, 493 (2006), hep-ph/0601169
12. F. Ambrosino et al. (KLOE), Eur. Phys. J. **C47**, 589 (2006), hep-ex/0604048
13. H. Czyz, A. Grzelinska, J.H. Kuhn, G. Rodrigo, Eur.Phys.J. **C39**, 411 (2005), hep-ph/0404078
14. F. Ambrosino et al. (KLOE Collaboration), Phys.Lett. **B670**, 285 (2009), 0809.3950
15. P. Lukin et al., http://www.lnf.infn.it/kloe2/tools/getfile.php?doc_fname=K2PD-6.pdf&doc_ftype=docs
16. B. Lautrup, A. Peterman, E. De Rafael, Nuovo Cim. **A1**, 238 (1971)

17. P. Fayet, Phys. Lett. **B95**, 285 (1980)

18. B. Batell, M. Pospelov, A. Ritz, Phys. Rev. **D80**, 095024 (2009), 0906.5614

19. N. Arkani-Hamed, N. Weiner, JHEP **12**, 104 (2008), 0810.0714

20. M. Pospelov, A. Ritz, M.B. Voloshin, Phys. Lett. **B662**, 53 (2008), 0711.4866

21. B. Holdom, Phys. Lett. **B166**, 196 (1986)

22. F. Archilli et al., Phys.Lett. **B706**, 251 (2012), 1110.0411

23. D. Babusci et al. (KLOE-2 Collaboration), Phys.Lett. **B720**, 111 (2013), 1210.3927